Journal Pre-proof

Electrochemical degradation of nanoplastics in water: Analysis of the role of reactive oxygen species

Marthe Kiendrebeogo, M.R. Karimi Estahbanati, Yassine Ouarda, Patrick Drogui, R.D. Tyagi

PII: S0048-9697(21)06973-4

DOI: https://doi.org/10.1016/j.scitotenv.2021.151897

Reference: STOTEN 151897

To appear in: *Science of the Total Environment*

Received date: 25 September 2021

Revised date: 14 November 2021

Accepted date: 19 November 2021

Please cite this article as: M. Kiendrebeogo, M.R.K. Estahbanati, Y. Ouarda, et al., Electrochemical degradation of nanoplastics in water: Analysis of the role of reactive oxygen species, *Science of the Total Environment* (2021), https://doi.org/10.1016/j.scitotenv.2021.151897

Electrochemical degradation of nanoplastics in water: Analysis of the role of reactive oxygen species

Marthe Kiendrebeogo[a], M.R. Karimi Estahbanati[a*], Yassine Ouarda[a], Patrick Drogui[a*], RD. Tyagi[b]

[a] Institut national de la recherche scientifique (INRS) - Centre Eau Terre Environnement (ETE), 490 rue de la Couronne, Québec (QC), CANADA, G1K 9A9

[b] Distinguished Prof Huzhou University, China, Chief Scientific Officer, BOSK Bioproducts, Québec, CANADA

*Corresponding authors: patrick.drogui@inrs.ca,

Mahmoodreza.Karimiestahbanati@inrs.ca.

Abstract

Microplastics and nanoplastics (NPs) are emerging water contaminants which have recently gained lots of attention because of their effects on the aquatic systems and human life. Most of the previous works on the treatment of plastic pollution in water have been focused on microplastics and a very limited study has been performed on the NPs treatment. In this work, the role of main reactive oxygen species (ROSs) in the electrooxidation (EO) and electro-peroxidation (EO-H_2O_2) of NPs in water is investigated. In-situ generation of hydroxyl radicals ($^{\bullet}OH$), persulfates ($S_2O_8^{2-}$), and hydrogen peroxide (H_2O_2) were performed using boron-doped diamond (BDD) as the anode, whereas titanium (in EO process) and carbon felt (CF, in EO-H_2O_2 process) were used as cathode. In the EO process, NPs were mainly oxidized by two types of ROSs on the BDD surface: (i) $^{\bullet}OH$ from water discharge and (ii) $SO_4^{\bullet-}$ via $S_2O_8^{2-}$ reaction with $^{\bullet}OH$. In EO-H_2O_2 process, NPs were additionally degraded by $^{\bullet}OH$ formed from H_2O_2 decomposition as well as $SO_4^{\bullet-}$ generated from direct or indirect reactions with H_2O_2. Analysis of the degradation of NPs showed that EO-H_2O_2 process was around 2.6 times

more effective than EO process. The optimum amount of NPs degradation efficiency of 86.8% was obtained using EO-H_2O_2 process at the current density of 36 mA.cm^{-2}, 0.03 M Na_2SO_4, pH of 2, and 40 min reaction time. In addition, 3D EEM fluorescence analysis confirmed the degradation of NPs. Finally, the economic analysis showed the treatment of NPs using EO-H_2O_2 process had an operating cost of 2.3 $US.m^{-3}, which was around 10 times less than the EO process. This study demonstrated the in-situ generation of ROSs can significantly enhance the degradation of NPs in water.

Keywords: Nanoplastic; polystyrene; water treatment; electrooxidation; H_2O_2 electrogeneration; degradation.

1. Introduction

Nanoplastics (NPs) have become a new emerging contaminant owing to their undeniable evidence occurrence due to bulk plastic degradation to form smaller particles down to the nanoscale (Cai et al., 2021; Ekvall et al., 2019), their difficulty in recycling (i.e. in biosolids) or elimination by conventional waste-water treatment technologies (Enfrin et al., 2019). NPs can be defined as a subgroup of plastics with an effective diameter less than 1,000 nm (da Costa et al., 2016; Gigault et al., 2018). Polymer nanoparticles that are produced intentionally for specific purposes such as cosmetic products (Hernandez et al., 2017) and synthetic microfibers (MFs) from the laundry of synthetic textile are important sources of microplastics (MPs) and NPs can enter the environment through wastewater treatment plants (De Villiers, 2019; Kelly et al., 2019). The concentration of NPs was estimated to be beyond 10^{14} times that of MPs in marine environments (Wang et al., 2020). Despite the vast presence of NPs in the environment, we are lacking harmonized and reliable methodologies for analyzing NPs in waters (Cai et al., 2021). Polystyrene (PS) is one of the most widely used plastics in real daily life (over 23 million tons per year), making it one of the most significant constituents of NPs (Lithner et al., 2011). On the other hand, the literature review demonstrated that PS is one of the most toxic polymers in the form of MPs and NPs (Karimi Estahbanati et al., 2021a).

The size of plastic particles is an important key in the connection with their toxicity in the waters because the smaller the plastic the bigger its capacity to absorb higher concentrations of contaminants (Liu et al., 2016). For example, NPs with a size of 50 nm can adsorb more toxic compounds than MPs around 10 µm in size (Ma et al., 2016). This may indirectly increase the exposure of Polycyclic Aromatic Hydrocarbons (PAHs) to organisms and thus increase their potential carcinogenic and mutagenic potency (White, 1986) as that is known for the properties of the styrene monomer (Lithner et al., 2011). In addition, NPs can enter into cells by endocytic pathways and accordingly cross the blood-brain barrier (Koziara et al., 2003), or penetrate the chorion of fish eggs (Kashiwada, 2006). Incineration of MPs and NPs aggregated in wastewater plant biosolids causes serious environmental problems due to the release of NPs. That increases direct exposure of PAHs to aquatic organisms (Liu et al., 2016) such as incineration by-products whose toxicity is still unrecognized (Miyake et al., 2017).

Current conventional sewage sludge treatment as lime stabilization and biological degradation causes the formation of smaller plastic particles (González-Pleiter et al., 2019; Mahon et al., 2017). That means the majority of biosolids used as agricultural fertilizer could threaten human health because of the high NPs content (Karimi Estahbanati et al., 2021c). Several methods have been tested for the upcycling of plastic waste that contributes to the reduction of environmental pollution by plastic particles (Karimi Estahbanati et al., 2021b). For example, microbial degradation of polymers got increasing attention from researchers (Ali et al., 2014; Paco et al., 2017), however, this method usually takes several weeks or even months to convert the plastics.

The pyrolysis of plastics is another approach for upcycling plastics particles to value-added products (i.e. fuel or chemical feedstock). However, the produced waste oil from this process may pollute the environment by the generation of contaminants like plastic particles (Miao et al., 2020).

The previous studies on the treatment of NPs in waters focused on their separation (Chen et al., 2021; Murray and Örmeci, 2020). Interestingly, only one article addressed the degradation of NPs using the photocatalytic process (Dominguez-Jaimes et al., 2021). Once again, this showed that it takes several days to achieve an NPs removal efficiency as previously demonstrated for MPs degradation (Ariza-Tarazona et al., 2019; Phonsy et al., 2015). On the other hand, aging of MPs proceeds at a very slow rate, causing a very long time for the degradation of the current environmental NPs pollution (Luo et al., 2021). However, studies have shown effective removal of MPs using electrochemical processes for hours' treatment time (Kiendrebeogo et al., 2021; Miao et al., 2020). Thus, it is very important to investigate electrochemical treatments for the degradation of NPs in waters in the order to prevent their accumulation in the sewage sludge and biosolids. Electrochemical advanced oxidation processes (EAOPs) generate diverse reactive oxygen species (ROSs) such as hydroxyl radical ($^{\bullet}OH$, E_0 = 2.8 V vs. NHE) and hydrogen peroxide (H_2O_2, E_0 = 1.8 V vs. NHE) at high concentrations. These processes have proven to be ecofriendly and effective ways for eliminating persistent contaminants in water (Miao et al., 2020). Sulfate radical ($SO_4^{\bullet-}$, E_0 = 2.6 V vs. NHE) is considered an important constituent of AOPs (Deng and Zhao, 2015; Wacławek et al., 2017) which exhibits a great capability for degradation of plastic particles (Kang et al., 2019). This

radical can be formed from $S_2O_8^{2-}$ activation via H_2O_2 (Hilles et al., 2015). During an electro-oxidation (EO) process, the $^{\bullet}OH$ can be formed at the anode from the oxidation of water. These radicals can also be formed in the bulk of solution using the continuous electro-generation of H_2O_2 from O_2 reduction (Zhou et al., 2018; Zhou et al., 2019).

Several studies reported that CF cathode is efficient in the generation of H_2O_2 in O_2-saturated solutions compared to other carbonaceous materials (Bañuelos et al., 2016; Cotillas et al., 2015; Garcia-Segura et al., 2012). H_2O_2 is electrogenerated from the two-electron reduction of O_2 on carbonaceous cathodes, such as carbon felt, vitreous carbon, O_2-diffusion electrodes, or graphite (Komtchou et al., 2015). Besides, (Guitaya et al., 2015) identified the best cathode material (carbon felt versus graphite felt) for H_2O_2 production. Carbon felt was more appropriate for H_2O_2 formation than graphite felt. After 60 min of electrolysis time, a concentration of 19.6×10^{-5} M was recorded with carbon felt, whereas 5.59×10^{-5} M was measured for graphite felt (a concentration three times lower). The amorphous structure of carbon felt facilitates the trapping of dissolved oxygen so that it can be reduced into H_2O_2, compared with the hexagonal structure of graphite felt which is less appropriate for oxygen trapping (Yue et al., 1990).

This paper studies the role of ROSs in the electrochemical degradation of NPs in water. In this regard, the effects of current density and Na_2SO_4 concentration on the concentration of in-situ electro-generated $^{\bullet}OH$ and $S_2O_8^{2-}$ using boron-doped diamond (BDD) were first investigated, respectively. In addition, the role of the carbon-felt (CF) cathode in the in-situ electro-generation of H_2O_2, as well as the effects of current density, air injection, and using one and two pieces of cathodes on the concentration of generated H_2O_2 were studied. Afterward, the effects of the concentration of Na_2SO_4, and the concentration of NPs on the rate of NPs degradation were evaluated. Total organic carbon (TOC) and three-dimensional excitation and emission matrix fluorescence (3D EEM) analyses were used to assess the mineralization and degradation of NPs. Finally, an economical study was performed on the electrochemical degradation of NPs in water.

2. Materials and methods

2.1. Chemicals and preparation of synthetic NPs effluents

The aqueous suspension of PS nanospheres (1% solids) with a diameter of 100 ± 4 nm and a coefficient of variation of 7.7% was provided by Thermo Scientific USA. The NPs synthetic solution was prepared by adding PS nanospheres at a concentration of 10 and 20 mg/L and sodium sulfate (Na_2SO_4) was used as a supporting electrolyte. Na_2SO_4 was an analytical grade reagent supplied by the Mat laboratory (Quebec, QC, Canada). Different concentrations of Na_2SO_4 (0.007, 0.030, and 0.060 M) were tested to assess its effect on treatment performances. All the NPs degradation experiments were performed by preparing spontaneously a new synthetic solution with a final volume of 1 L from which 800 or 900 mL was used. RNO (N, N-Dimethyl-4-nitroso-aniline, $C_2H_6N_2O$, 97%) supplied by Sigma Aldrich was used as a probe molecule to assess the production of $^{\bullet}OH$ during electrolysis. The RNO stock solution was prepared by dissolving 49.4 mg/L of RNO in 1 L of a buffer solution consisting of anhydrous dibasic sodium phosphate (99%) crystalline monobasic potassium phosphate (99%). The buffer solution was adjusted to pH 7. H_2O_2 (30%) used for the calibration curve was analytical grade from Sigma Aldrich.

2.2. Electrolytic setups

The electrochemical treatment of NPs was carried out in the batch mode with niobium-covered boron-doped-diamond (Nb/BDD) as anode and titanium (Ti) or CF as the cathode. The reactor was made of Plexiglas with a dimension of 14.5 cm (length) × 6.4 cm (width) × 17.7 cm (height). Accordingly, three types of electrode combination (anode-cathode) were employed to conduct the experiments: (i) Ti-BDD, (ii) CF-BDD, and (iii) CF-BDD-CF. The distance between electrodes was 1.0 cm. Ti and BDD electrodes were grid and circular shape with a diameter of 12 cm, a thickness of 0.1 cm, and a surface area of 113 cm^2. The CF electrode was made of 10-20 μm interwoven fibers and had an 11 cm (length) × 9 cm (width) main side rectangular shape and a thickness of 1 cm. CF consisted of 99.00 to 99.70% of carbon and 0.02 to 0.25% of ashes. The Anodes and cathodes were connected respectively to the positive and negative outlets of a digital DC generator model 382275 (EXTECH Instruments, Montréal, Canada) with a

maximum current supply of 20 A at an open circuit potential of 30 V. In some experiments the system was fed with 900 mL.min^{-1} of compressed atmospheric air injection into the reactor to saturate continuously the solution subjected to the treatment with oxygen. During electrolysis, the solution was mixed using a magnetic stirrer and air bubbling.

2.3. Experimental procedure

The degradation of NPs was conducted using two different oxidation processes: (i) EO using an electrochemical reactor comprising of Ti (cathode) and BDD (anode) on which $^{\bullet}OH$ was formed (Configuration Ti-BDD); (ii) EO with in-situ H_2O_2 generation (EO-H_2O_2 process) consisted in treating NPs using an electrochemical reactor comprising of BDD (anode) and CF (cathode) on which H_2O_2 was formed (configuration CF-BDD). The first sets of electrochemical oxidation experiments were focused on evaluating the potential of ROS production. During these tests, the concentration of ROS (including $^{\bullet}OH$, H_2O_2, and $S_2O_8^{2-}$) was measured to investigate their contribution to the NPs oxidation. The production of $^{\bullet}OH$ by BDD anode was measured at the current densities of 36, 72, and 108 mA.cm^{-2}, and the generation of H_2O_2 by CF cathode was evaluated at current densities of 6, 12, and 36 mA.cm^{-2} (i.e., 0.5 to 3.0 A). In addition, the effect of $S_2O_8^{2-}/H_2O_2$ activation during the EO-H_2O_2 process was analyzed. During these tests, the degradation of NPs was analyzed by TOC, UV-vis spectrophotometry, and 3D EEM techniques to evaluate the performance of different electrochemical oxidation processes.

2.4. Analysis techniques

2.4.1. Hydroxyl radical concentration measurements

The production of $^{\bullet}OH$ was estimated by its reaction with RNO according to the method reported by (García-Gómez et al., 2014). RNO is an organic dye that is bleached selectively by oxidation with $^{\bullet}OH$ and does not react with single oxygen, superoxide anions (O_2^{-}), or other peroxy compounds (Muff et al., 2011; Simonsen et al., 2010). To measure the amount of generated $^{\bullet}OH$ during the EO experiments, the amount of removed RNO was monitored by the measurement of absorbance band at 440 nm using a

UV-visible spectrophotometer (UV 0811 M136, Varian, Australia. The RNO calibration curve was obtained by plotting the RNO absorbance as a function of RNO concentration (from 0 to 5.81× 10^{-5} M). The rate of $^{\bullet}OH$ production is equal to the rate of RNO disappearance by the assumption of the first-order reaction, according to Eq. (1):

$$V = \frac{dC}{dt} = -kC \quad (1)$$

where *V*, *C*, *k*, and *t* correspond to the production rate of $^{\bullet}OH$, the RNO concentration, the first-order reaction rate constant, and the reaction time, respectively. The integration of Eq. (1) gives:

$$Ln(\frac{Co}{C}) = kt \quad (2)$$

where C_0 and C_t are the initial concentration of RNO and the concentration of RNO at time t. The value of *k* could be calculated from the slope of a plot of *t* versus $Ln(C_0/C)$ in Eq. (2).

2.4.2. Peroxydisulfate concentration measurements

The Wessler method was used to measure the concentration of peroxydisulfate ($S_2O_8^{2-}$) through the oxidation of iodide ions (I^-) into iodine (I_2) (Ishibashi et al., 2000; Xiang et al., 2011). When an oxidizing agent like $S_2O_8^{2-}$ is present in the solution, I^- ions are oxidized to give I_2 (see Eq. (3)). Subsequently, I_2 reacts with I^- present in excess in the solution to form tri-iodide (I_3^-) ion according to Eq. (4) (Entezari and Kruus, 1994). The Wessler method is based on the direct titration of I_2 produced from the oxidation of I^-:

$$S_2O_8^{2-} + 2I^- \rightarrow 2SO_4^{2-} + I_2 \quad (3)$$

$$I_2 + I^- \leftrightarrow I_3^- \quad (4)$$

I_3^- is analyzed by absorbance measurements at 353 nm (Koda et al., 2003). To do so, samples were taken and diluted 4 times at different reaction times (0 to 180 min). From the diluted solution, 10 ml was mixed with an excess of potassium iodide (500 mg). The

mixture was allowed to react for 15 min while stirring. Then, the obtained solution was analyzed at 353 nm using a UV-vis spectrophotometer (Carry UV 50, Varian Canada).

2.4.3. H_2O_2 concentration measurement

The volumetric dosage method (Sigler and MAster, 1957) was used to measure H_2O_2 concentration. Under acidic conditions (H_2SO_4, 9 N), a 5.88×10^{-3} M cerium solution ($Ce(SO_4)_2$, $2(NH_4)_2$ SO_4,$2H_2O$) was used for the titration of the sample that was mixed with three drops of $Fe(O\text{-phen})_3^{2+}$ as an indicator. The gradual change of the solution color from red to blue indicated the total oxidation of H_2O_2 using the cerium solution. To quantitatively determine the concentration of H_2O_2, a calibration curve was obtained by plotting the cerium volume as a function of H_2O_2 concentration (from 0 to 2.06 M corresponding 0 to 70 mg/L).

2.4.4. NPs concentration measurement

The concentration of NPs in the solution was determined by the spectrophotometric spectral absorption measurements of C=C bonds of PS at 254 nm. A calibration curve of NPs versus relative absorbance was used to calculate the residual NPs concentration and define the degradation efficiency. The removal efficiency was accordingly calculated according to Eq. (5):

$$Degradation\ efficiency\ (\%) = \frac{C_0 - C_t}{C_0} \times 100 \quad (5)$$

where C_o and C_t are the initial and final concentrations of NPs in the sample, respectively.

To evaluate the obtained results from the spectrophotometric analysis, the NPs degradation was also measured based on TOC analysis. To do so, the samples were analyzed using a Shimadzu TOC 5000A analyzer (Shimadzu Scientific Instruments, Kyoto, Japan).

2.4.5. 3D EEM analysis

To decompose the fluorescence components in the NPs samples and track dissolved organic matter evolution during treatment, 3D EEM analysis was performed using Varian

Cary Eclipse Fluorescence Spectrophotometer (USA). Emission scans were performed from 230 to 600 nm at 5 nm increments, with excitation wavelengths from 220 to 650 nm at 5 nm intervals. The scanning rate was maintained at 1,200 nm/min. The slit widths for excitation and emission were 10 nm. A 290 nm emission cut-off filter was used in scanning to eliminate second-order Raleigh light scattering.

2.5. Energy consumption analysis

Energy consumption is an important factor concerning EAOPs. Eq. (6) was employed to express that in kWh.m^{-3}:

$$EC\ (kWh \cdot m^{-3}) = \frac{T \times I \times t}{V} \tag{6}$$

where *T*, *I*, *t*, and *V* represent the average cell voltage (V), the applied current (A), the duration of electrolysis (h), and the volume of treated water (m^3).

The operating cost was estimated considering energy consumption and electrolyte costs. The cost of electricity and electrolyte was estimated based on a unit cost of 0.06 $US/kWh and 0.3 $US/kg for Na_2SO_4 (industrial grade).

3. Results and discussion

3.1. In-situ ROS production

The performance of electrochemical processes in the degradation and mineralization of organic pollutants are related to the amount of in-situ electro-generated ROSs (Daghrir et al., 2013; Komtchou et al., 2015; Sanni et al., 2021). Accordingly, some tests were conducted to evaluate the efficacy of the electrolytic cell to produce $^{\bullet}OH$, H_2O_2, and $S_2O_8^{2-}$. According to previous studies, BDD anode is the only non-active electrode capable of oxidizing the sulfate (SO_4^{2-}) to persulfate ($S_2O_8^{2-}$) which can contribute to oxidizing organic compounds when Na_2SO_4 is used as a supporting electrolyte (Canizares et al., 2005; Serrano et al., 2002). In addition, using CF as the cathode is more appropriate than carbon-graphite for H_2O_2 formation (Guitaya et al., 2015; Khataee et al., 2011; Komtchou et al., 2015). Consequently, the combination of BDD anode and CF cathode was used for the analysis of ROSs electro-generation and their potential in the

degradation of NPs. In the following sub-sections, the potential of BDD anode in the generation of $^{\bullet}OH$ and $S_2O_8^{2-}$ as well as CF cathode in the production of H_2O_2 are analyzed.

3.1.1. Electrochemical generation of hydroxyl radicals and persulfates

In this study, the evaluation of $^{\bullet}OH$ production was carried out by following the bleaching of RNO by $^{\bullet}OH$ during the EO process with the selected electrode set (Nb/BDD). Fig. 1 depicts the concentration of generated $^{\bullet}OH$ and $S_2O_8^{2-}$ through time. Fig. 1a illustrates the $^{\bullet}OH$ generated in the absence of NPs at different current densities of 36, 72, and 108 mA.cm^{-2}. The inset panel of Fig. 1a shows the RNO disappearance rate following a first-order kinetic model. As observed from these results, the amount of $^{\bullet}OH$ increases with electrolysis time and current density. In addition, the $^{\bullet}OH$ formation obeys the first-order kinetic with the rate constant (k) of 0.0861, 0.1472, and 0.2150 min^{-1} for 36, 72, and 108 mA.cm^{-2}, respectively. Total removal of RNO (8 mg/L) was obtained after 20 and 30 min for 72 and 108 mA.cm^{-2}, respectively, while it took over 30 min for 36 mA.cm^{-2}. In addition, it can be seen from Fig. 1a that the $^{\bullet}OH$ production rate reached 0.39, 0.75, and 1.11 × 10^{-5} M.min^{-1} after 20 min electrolysis time for 36, 72, and 108 mA.cm^{-2}, respectively. A relatively high rate of $^{\bullet}OH$ production (1.11 × 10^{-5} M.min^{-1}) was recorded in our study using BDD/Nb electrodes and 108 mA.cm^{-2} current density compared to the study where the production rate was 0.4 × 10^{-5} M.min^{-1} after 20 min of electrolysis time under different operating conditions (Ti/PbO_2 anode, current density of 67 mA.cm^{-2} and recirculation flow rate 232 ml.min^{-1}) (García-Gómez et al., 2014). Several authors consider BDD as the electrode of choice for efficient and complete degradation of refractory pollutants (Martínez-Huitle and Panizza, 2018). Indeed, many studies mentioned that the interaction between $^{\bullet}OH$ and the surface of BDD anodes is considered to be very weak resulting in a much greater O_2 overvoltage than the other anodes such as platinum and lead dioxide (PbO_2), iridium (IV) oxide (IrO_2) (Ciríaco et al., 2009; Ignasi et al., 2008; Martínez-Huitle et al., 2004; Yassine et al., 2018).

$S_2O_8^{2-}$ generation was analyzed in the absence of NPs at two different initial Na_2SO_4 concentrations (i.e. 0.03 and 0.06 M) and at a pH of 5 using the current density of 108 mA.cm^{-2} for 180 min electrolysis time. As shown in Fig. 1c, $S_2O_8^{2-}$ production after 180

min enhanced from 0.48 to 0.72 mM by increasing the Na_2SO_4 concentration from 0.03 to 0.06 M. However, by applying a lower current intensity the $S_2O_8^{2-}$ generation decreased. For example, at 36 mA.cm^{-2} (67% reduction at current density) and 0.06 M Na_2SO_4, the $S_2O_8^{2-}$ concentration reduced to 0.19 mM (73% reduction), which shows a significant effect of the current density on the $S_2O_8^{2-}$ generation (the data are not shown in Fig. 1b). Previous studies also reported the generation of $S_2O_8^{2-}$ by BDD anode via various ways: (i) direct oxidation of SO_4^{2-} by electron transfer according to Eq. (7) (Davis et al., 2014; Serrano et al., 2002; Smit and Hoogland, 1971a; Smit and Hoogland, 1971b), (ii) indirect oxidation of SO_4^{2-} by BDD($^{\bullet}$OH) (Eq. (8)) (Barreto et al., 2015; Ganiyu and Martínez- Huitle, 2019; Serrano et al., 2002), and (iii) recombination of principal intermediate ($SO_4^{\bullet-}$ species) on the anode surface during indirect oxidation (Eq. (9)) (Barreto et al., 2015; Ganiyu and Martínez- Huitle, 2019).

$$2SO_4^{2-} \rightarrow S_2O_8^{2-} + 2e^- \quad (7)$$

$$2HSO_4^- + 2BDD(OH^{\bullet}) \rightarrow S_2O_8^{2-} + 2H_2O \quad (8)$$

$$SO_4^{\bullet-} + SO_4^{\bullet-} \rightarrow S_2O_8^{2-} \quad (9)$$

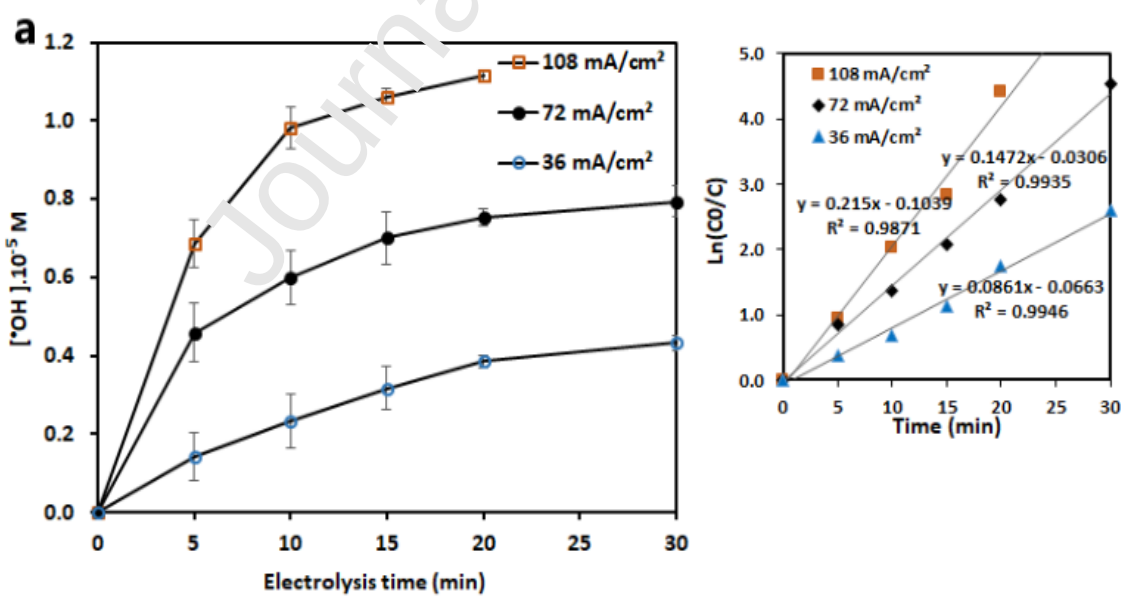

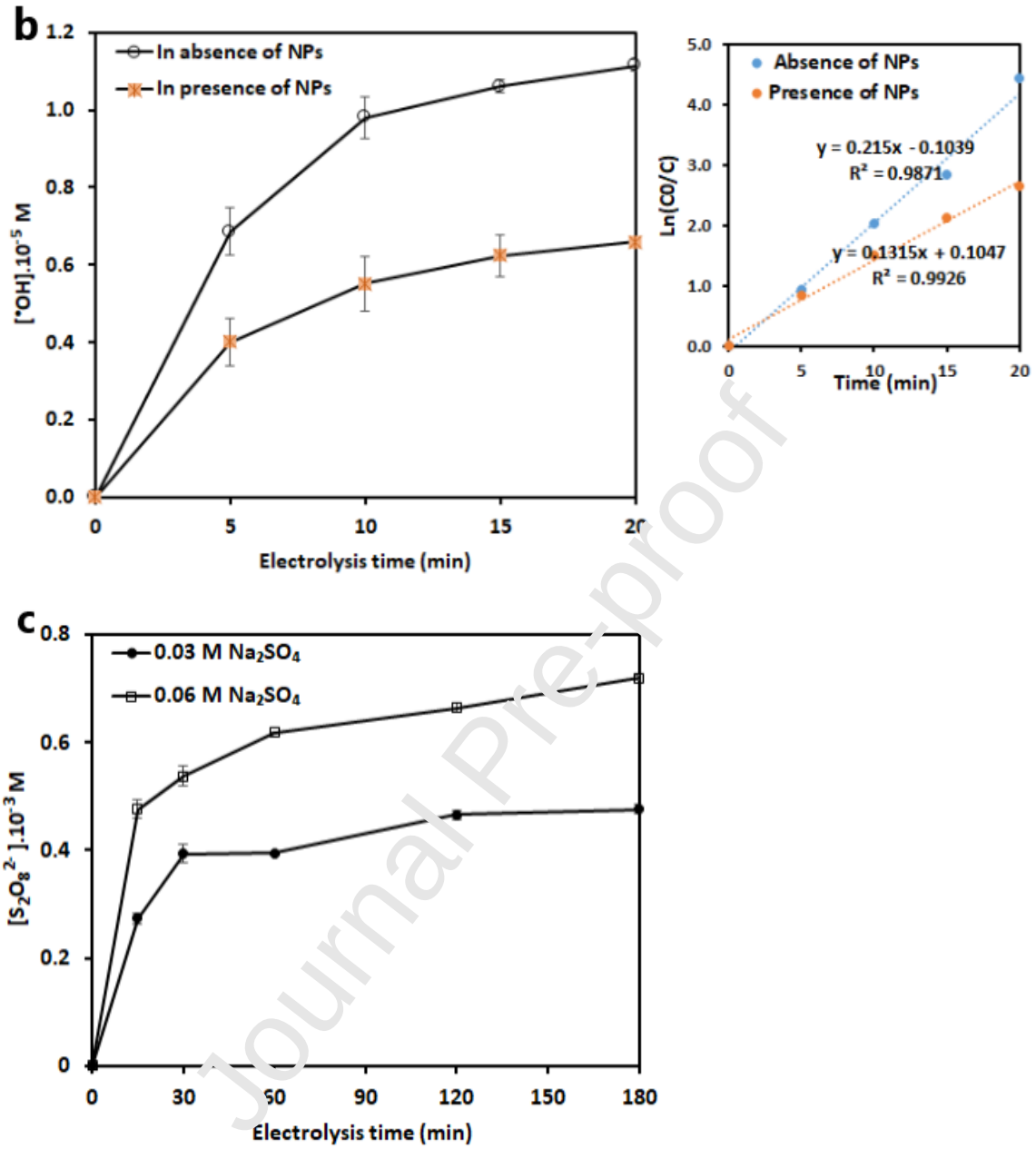

Fig. 1. Analysis of simultaneous production of ROSs in the absence and presence of NPs a) $^{\bullet}OH$ at different current densities in the absence of NPs, b) Effect of the presence of NPs on the concentration of $^{\bullet}OH$ during the electrolysis, the inset figures represent the first-order reaction kinetics analysis of RNO. $[Na_2SO_4]$ = 0.03 M. c) $S_2O_8^{2-}$ at the current density of 108 $mA.cm^{-2}$.

3.1.2. Electrochemical generation of H_2O_2

To investigate the performance of CF cathode to produce H_2O_2, several experiments were performed in the absence of NPs with 1.0 g/L Na_2SO_4 (as supporting electrolyte) at an initial pH of 5. These experiments were conducted at the current densities of 6, 12, and 36 mA.cm^{-2} using two CF cathodes and in the continuous injection of air to assure oxygen saturation. The H_2O_2 concentration in the solution at different reaction times and current densities are illustrated in Fig. 2a. As it can be seen, the H_2O_2 concentration increased significantly up to 30 min and reached around 0.14 $\pm$ 0.013, 0.13 $\pm$ 0.01, 0.14 $\pm$ 0.04 M for 6, 12, and 36 mA.cm^{-2}, respectively then decreased slightly until 1 hour. This behavior has been also reported by previous studies (Li et al., 2020; Salmerón et al., 2019). It can also be seen from Fig. 2a that the current density has no significant effect on the H_2O_2 concentration produced during electrolysis. In addition, the concentration of H_2O_2 has fluctuated a lot after 30 min of electrolysis. This is due to parasitic reactions that can take place in the cell (Salmerón et al., 2019). There may be an electrochemical reduction of H_2O_2 continuously accumulated in the solution at the cathode following the Eq. (10). This explains the spontaneous variation of its concentration over time.

$$H_2O_2 + 2H^+ + 2^+ \rightarrow 2H_2O \quad (10)$$

In addition, the presence of BDD in the undivided cell could promote the oxidation of H_2O_2 at the surface of the anode (Eqs. (11)-(12)) and its decomposition in the electrolysis medium according to Eq. (13) (Özcan et al., 2008).

$$H_2O_2 \rightarrow HO_2^{\bullet} + H^+ + e^- \quad (11)$$

$$HO_2^{\bullet} \rightarrow O_2 + H^+ + e^- \quad (12)$$

$$H_2O_2 \rightarrow H_2O + 1/2O_2 \quad (13)$$

Furthermore, the temperature measured during electrolysis time increased from 20 ± 1.2 to 40 ± 3.4 ºC. That did not favor the stabilization of H_2O_2. It has been shown by (Badellino et al., 2006) that by reducing the temperature from 18 to 10 ºC, the final concentration of H_2O_2 can be increased three times. This can be explained by the

decrease in the solubility of oxygen and the increase in H_2O_2 dissociation under high temperatures (Badellino et al., 2006; Özcan et al., 2008).

Fig. 2b shows the effects of the number of cathodes and air injection on H_2O_2 production. As expected, the concentration of generated H_2O_2 is significantly higher when using two cathodes in comparison to one cathode, especially in the presence of air injection. In addition, it is inferred from this figure that the air injection can enhance H_2O_2 generation in both cases of using one or two cathodes. Comparing these results with the maximum H_2O_2 concentration of 1.44 mg/L that was obtained at a previous study by (Komtchou et al., 2015) using 17.7 mA.cm^{-2} current density and with 112 cm^2 CF surface area, confirms that the surface area of CF and O_2 saturation promotes the production of H_2O_2.

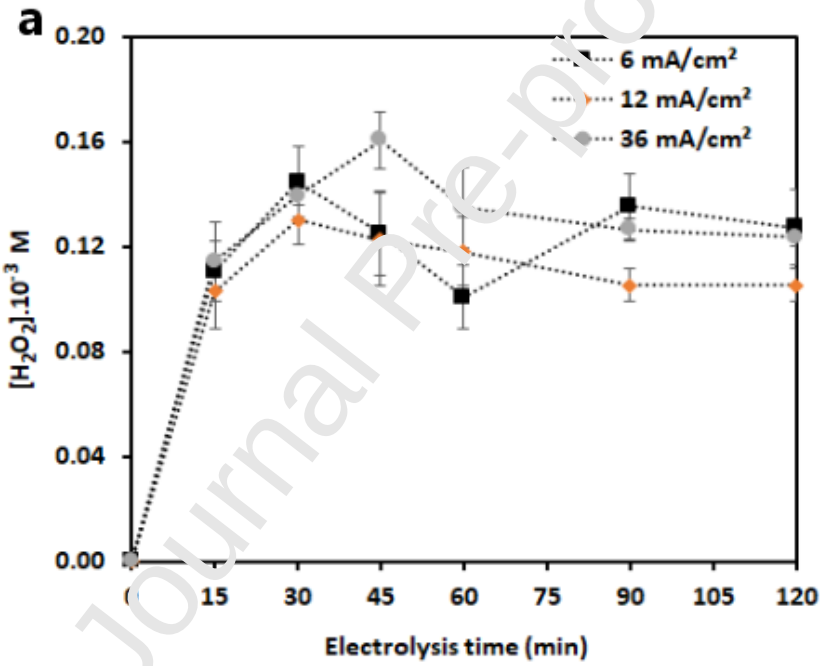

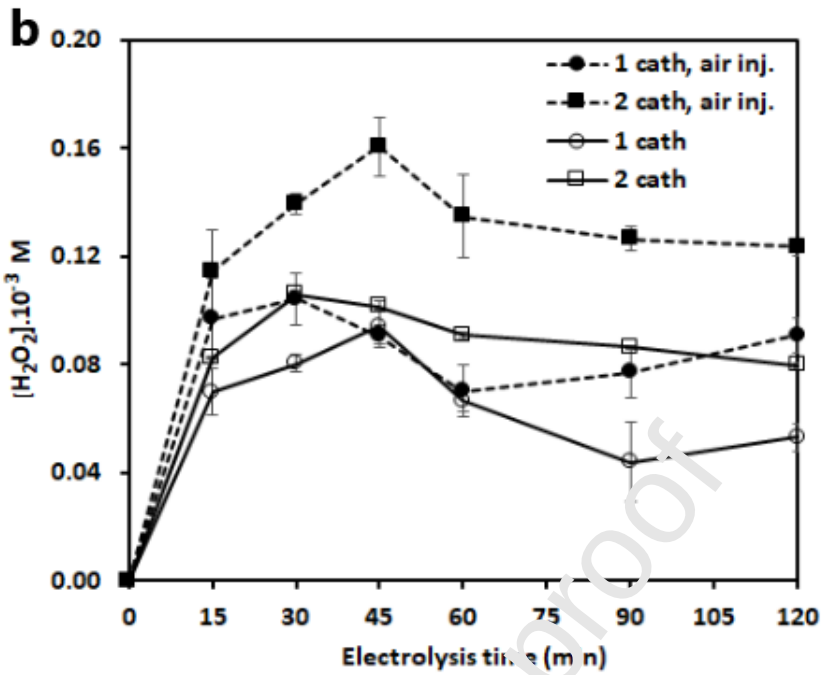

Fig.2. H_2O_2 production at different reaction time a) at different current densities using 2 cathodes with air injection, and b) with/without air injection and at a different number of cathodes.

3.2. Hydroxyl radical's contribution and NPs degradation kinetics

3.2.1. Hydroxyl radical contribution

After evaluating the production of $^{\bullet}OH$ radicals in the absence of NPs, the amount of $^{\bullet}OH$ was also tracked in the presence of NPs using a synthetically contaminated solution with 10 mg/L NPs. By comparing the amount of $^{\bullet}OH$ electrogenerated in the presence and absence of 10 mg/L of NPs for a current density of 108 $mA.cm^{-2}$, it can be seen clearly that the $^{\bullet}OH$ concentration decreased by almost 50% (Fig. 1b). $^{\bullet}OH$ production decreased from 0.7×10^{-5} to 0.4×10^{-5} M and 1.1×10^{-5} to 0.6×10^{-5} M after 5 and 20 min of electrolysis, respectively. This would mean that a fraction of the electrogenerated $^{\bullet}OH$ is used for NPs degradation. It's known that ROSs react favorably with electron-rich compounds (Stichnothe et al., 2002). For the case of PS NPs, $^{\bullet}OH$ reacted with the carbon double bonds (–C=C–) and attacked the aromatic nucleus, which is the major component of PS molecular.

3.2.2. Kinetic study of NPs degradation by EO process

It is known that the concentration of ROSs influences the performance of EAOPs in the degradation of pollutants (Komtchou et al., 2015; Özcan et al., 2008). To analyze that for NPs, the concentration of NPs during the EO process was measured at different current densities (36, 72, and 108 mA.cm^{-2}). These experiments were conducted using BDD anode and Ti cathode and in the presence of 0.03 M Na_2SO_4 and initial NPs concentration of 10 mg/L for 360 min. The initial and final pH values were 5.3 ± 0.3 and 9.5 ± 0.6, respectively. Fig. 3 shows the percentage of NPs removal changes depending on the current density imposed. The increase of current density from 36 to 72 mA.cm^{-2} improved the degradation efficiency by around 20%, whereas an increase of current density up to 108 mA.cm^{-2} had no positive effect. The major electrogenerated ROSs involved in NPs degradation during the EO process include BDD($^{\bullet}$OH) produced directly at BDD surface from water discharge (Eq. (14)) (Panizza and Cerisola, 2005) and indirectly through the reaction between $S_2O_8^{2-}$ and BDD($^{\bullet}$OH) according to Eq. (15) (Dos Santos et al., 2020). Previous studies reported $S_2O_8^{2-}$ (E^0 = 2.08 V) capacity to oxidize and modify the organic molecules (Canizares et al., 2005; Marselli et al., 2003). To observe the sole effect of $S_2O_8^{2-}$ on NPs degradation, NPs were added into the final solution of a test that was performed at 0.19 mM $S_2O_8^{2-}$ using BDD at 36 mA.cm^{-2} to obtain a final NPs concentration of 10 mg/L. The solution was stirred for 120 min and NPs concentration was monitored. The results showed that the NPs concentration was constant after 120 min. Consequently, the sole presence of $S_2O_8^{2-}$ in our conditions does not degrade NPs, which is similar to the results obtained by (García-Gómez et al., 2014).

$$BDD + H_2O \rightarrow BDD(OH^{\bullet}) + H^+ + e^- \quad (14)$$

$$S_2O_8^{2-} + BDD(OH^{\bullet}) \rightarrow BDD + HSO_4^- + SO_4^{\bullet -} + 1/2O_2 \quad (15)$$

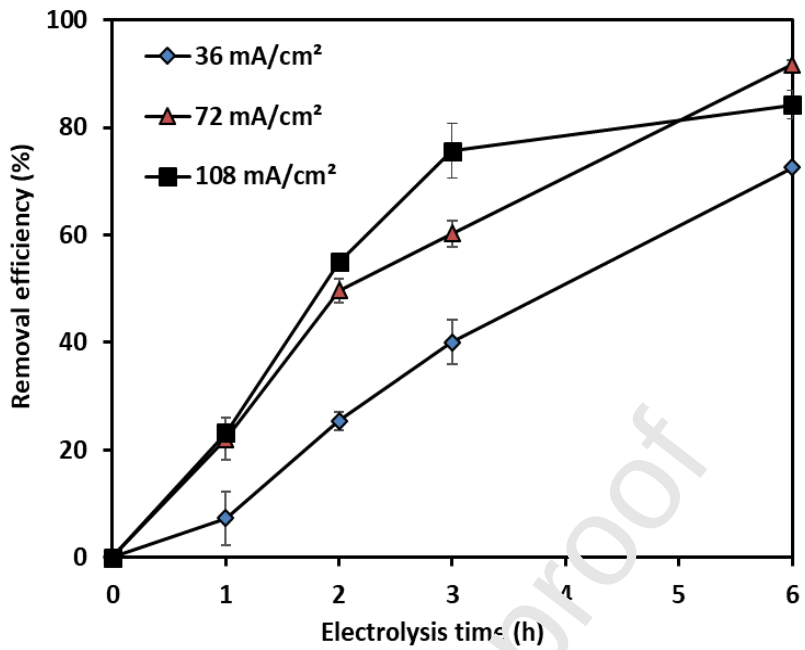

Fig. 3. Influence of applied current density on the degradation rate of NPs during EO treatment. Cathode = Ti, anode = BDD anode, $[NPs]_0$ = 10 mg/L, $[Na_2SO_4]$ = 0.03 M, volume = 900 mL.

The obtained results were used to develop pseudo-first-order and pseudo-second-order kinetic models. The pseudo-first-order kinetic model is described by Eq. (16):

$$Ln(\frac{Co}{C}) = k_1 t \quad (16)$$

where C_0, C, and k_1 represent the initial concentration of NPs, the concentration of NPs at time t, the first-order reaction rate constant (min^{-1}).

For the pseudo-second-order kinetic model, the equation described below was applied:

$$\frac{1}{C} - \frac{1}{C0} = k_2 t \quad (17)$$

where k_2 and t are the second-order reaction rate constant ($L.mg^{-1}\ min^{-1}$) and the reaction time, respectively.

The regression coefficient (R^2) was used for the selection of the most suitable model.

The calculated values of k_1, k_2, and R^2 obtained at different applied current densities are summarized in Table 1.

Table 1: Apparent rate constants as well as their R^2 for the oxidation of NPs by EO process at different applied current intensities under conditions described in Fig. 3b.

Cell	**[NPs] mg/L**	**Current density ($mA.cm^{-2}$)**	**Pseudo-first-order**		**Pseudo-second order**	
			k_1	R^2	k_2	R^2
Ti cathode/BDD anode	10	36	0.2235	0.9802	0.0456	0.8608
	10	72	0.4202	0.9809	0.0905	0.9668
	10	108	0.3211	0.9196	0.189	0.9243

In general, the R^2 of the pseudo-first-order kinetic model is relatively higher than that of the pseudo-second-order kinetic model, which shows that the first-order kinetic model describes very well the degradation of NPs by the EO process. In addition, it can be seen that k_1 values were decreased from 0.4202 to 0.3211 min^{-1} although increasing current density from 72 and 108 $mA.cm^{-2}$. Indeed, while imposing a current density of 108 $mA.cm^{-2}$, secondary reactions (such as the oxygen evolution) occurred significantly (Martinez-Huitle et al., 2015) or a fraction of $^{\bullet}OH$ produced was possibly wasted in the reaction of recombination (Martinez-Huitle et al., 2015). Therefore, it can be considered that 108 $mA.cm^{-2}$ was higher than the current density that was corresponding to the diffusion limitation.

3.3. Contribution of hydrogen peroxide in NPs degradation

The contribution of H_2O_2 in the degradation of NPs was analyzed during the EO process. To do so, CF was employed for the in-situ generation of H_2O_2. The experiments were conducted with 0.9 L/min air injection, 36 $mA.cm^{-2}$ anode current density, 1 g/L Na_2SO_4, 6 h electrolysis time, and 10 mg/L initial concentration of NPs. The use of one piece of CF cathode was compared to the use of two pieces of CF cathodes. The initial and final pH values were 5.1 ± 0.1 and 2.5 ± 0.0, respectively. As it can be seen in Fig. 4, using CF cathode the removal efficiency of NPs was 42 ± 0.2% after 60 min of electrolysis, while it was only 16.2 ± 1.9% using Ti as the cathode. It should be mentioned that the

improvement in removal efficiency using CF cathode compared to Ti could be expected if the concentration of H_2O_2 was higher (Badellino et al., 2006). To evaluate the sole effect of H_2O_2 in the degradation of NPs, 0.14× 10^{-3} M stabilized H_2O_2 solution (high amount based on Fig. 2) was prepared and NPs added to obtain a final concentration of 10 mg/L NPs at pH of 2. The analysis of the concentration of NPs showed that H_2O_2 injection could not induce NPs degradation (data not shown). Consequently, the high rate of NPs removal recorded in the experiments could be attributed to the regeneration of $SO_4^{\bullet-}$ in the solution by the activation of electrogenerated $S_2O_8^{2-}$ (Eqs. (7)-(9)) via EO-H_2O_2 through (i) direct reaction between $S_2O_8^{2-}$ and electrogenerated H_2O_2 at air diffusion cathode according to Eq. (18), (ii) indirect reaction between $S_2O_8^{2-}$ and $^{\bullet}OH$ from H_2O_2 dissociation due to the increase in the temperature of medium from 25 ºC to 45 ºC (Eq. (19)), and (iii) cathodic reduction based on Eq. (20) (Divyapriya and Nidheesh, 2021; Dos Santos et al., 2020; Hilles et al., 2016; Lin et al., 2016; Niu et al., 2020). Moreover, according to Eq. (18), during the regeneration of $SO_4^{\bullet-}$, $^{\bullet}OH$ was also produced simultaneously in the solution and contributed to the enhancement of the performance of the treatment system. It was shown in the literature that the reduction potential of $SO_4^{\bullet-}$ (E^0 = 2.6 V) is slightly lower than $^{\bullet}OH$ (E^0 = 2.8 V) (Fan et al., 2014); therefore $SO_4^{\bullet-}$ can attack a vast range of aromatic and cyclic organic molecules (Deng and Ezyske, 2011; Matta et al., 2010; Wojnarovits and Takacs, 2019). Consequently, NPs were oxidized simultaneously through $^{\bullet}OH$ addition to unsaturated bonds and H-abstraction as well as $SO_4^{\bullet-}$ electron transfer (Cai et al., 2018; Lan et al., 2017). It is reported in the literature that both the radicals represent comparable oxidation rates, however, the $SO_4^{\bullet-}$ mediated oxidation is more effective than the $^{\bullet}OH$-mediated one because of its electrophilic character and longer half-life (Divyapriya and Nidheesh, 2021; Lan et al., 2017; Nidheesh and Rajan, 2016). In another work, it was shown that $SO_4^{\bullet-}$ can effectively degrade cosmetic polyethylene MPs (Kang et al., 2019).

Another contribution of H_2O_2 in EO-H_2O_2 process efficiency consisted in the regeneration of SO_4^{2-} ions by reaction between H_2O_2 and $SO_4^{\bullet-}$ as per Eqs. (21)-(22) (Lin et al., 2016). This can explain why the pH of the solution during EO-H_2O_2 experiments decreased from 5 to 2 (Eqs. (22) and (23)). Thus, $SO_4^{\bullet-}$ and $^{\bullet}OH$ could be regenerated continuously by the conversion of $SO_4^{\bullet-}$ and $S_2O_8^{2-}$ in the solution. However, during the

EO process, the regeneration of SO_4^{2-} ions is not possible. During EO experiments (Fig. 3) the pH increased from 5 to 9. That can be explained by the reaction of added SO_4^{2-} with $^{\bullet}OH$ (Eq. (23)) (Durán et al., 2018; Tsitonaki et al., 2010).

$$S_2O_8^{2-} + H_2O_2 \rightarrow 2SO_4^{\bullet -} + 2OH^{\bullet} \quad (18)$$

$$S_2O_8^{2-} + OH^{\bullet} \rightarrow HSO_4^{-} + SO_4^{\bullet -} + 1/2\, O_2 \quad (19)$$

$$S_2O_8^{2-} + e^{-} \rightarrow SO_4^{\bullet -} + SO_4^{2-} \quad (20)$$

$$H_2O_2 + SO_4^{\bullet -} \rightarrow SO_4^{2-} + HO_2^{\bullet} + H^{+} \quad (21)$$

$$SO_4^{\bullet -} + HO_2^{\bullet} \rightarrow SO_4^{2-} + H^{+} + O_2 \quad (22)$$

$$SO_4^{2-} + OH^{\bullet} \rightarrow SO_4^{\bullet -} + OH^{-} \quad (23)$$

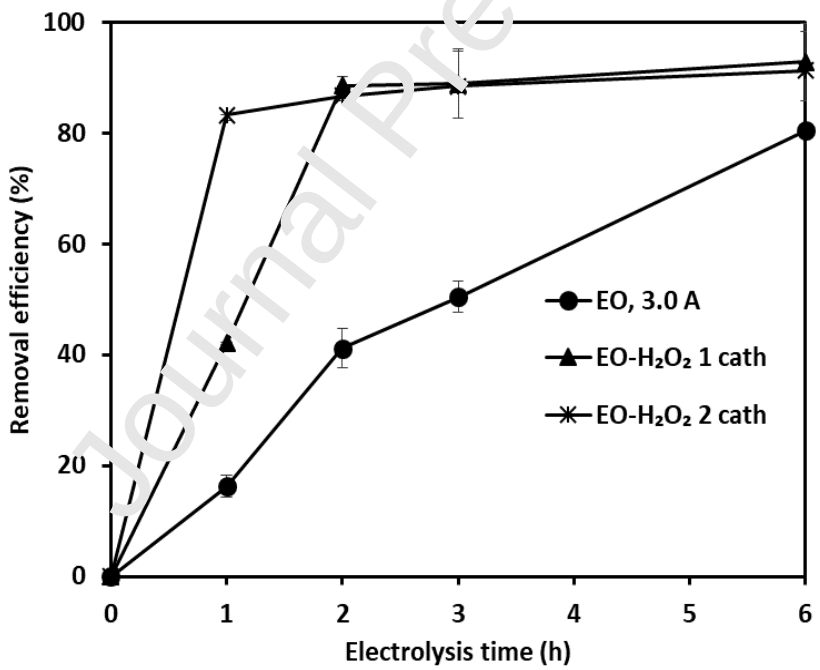

Fig. 4. Degradation of NPs during the electrolysis by EO and EO-H_2O_2 processes using Ti-BDD configuration for EO, CF-BDD and CF-BDD-CF configuration for EO-H_2O_2. $[NPs]_0$ = 10 mg/L, $[Na_2SO_4]$ = 0.007 M, current density = 36 mA.cm^{-2}, volume = 800 mL, initial pH = 5.1 ± 0.1, final pH = 2.5 ± 0.0.

3.4. Mineralization of NPs

Through the degradation of bio-refractory compounds by EAOPs, numerous by-products would be formed (Sires et al., 2014). To verify the performance for processes to further oxidize NPs until complete mineralization to water and carbon dioxide, the residual TOC of the samples was measured. The TOC of the samples treated by EO and EO-H_2O_2 are compared in Fig. 5. The initial TOC was 8.79 ± 0.44 mg/L, while at the end of treatment is reduced to 3.85 ± 0.41, 3.18 ± 0.24, and 2.08 ± 0.76 mg/L in EO, EO-H_2O_2 using one piece of the cathode, and EO-H_2O_2 using 2 pieces of cathodes processes, respectively. It can be concluded from these results that 23.5% of NPs transformed into by-products which were difficult to mineralize. Based on Fig. 5, the TOC removal efficiency after 6 h of electrolysis was 56.2 ± 4.6%, 63.8 ± 2.7%, and 76.3 ± 8.6% for EO, EO-H_2O_2 using one piece of the cathode, EO-H_2O_2 using 2 pieces of cathodes processes, respectively. Nevertheless, the corresponding NPs removal efficiencies were 80.4 ± 2.23%, 92.8 ± 6.3%, and 91.26 ± 3.04%, respectively (see Fig. 4).

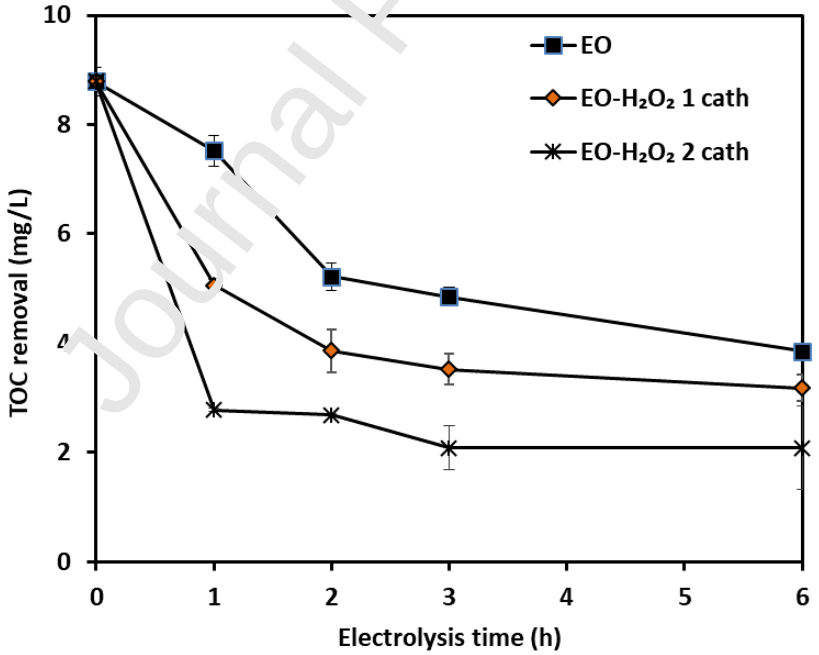

Fig. 5. TOC removal during the electrolysis time for the mineralization of NPs using EO and EO-H_2O_2 processes. The experimental conditions are similar to Fig. 4.

3.5. Effect of electrogenerated persulfates concentration

Additional experiments were conducted to determine the best operating conditions during the treatment of NP-containing effluent using the EO-H_2O_2 process. Since the $S_2O_8^{2-}$ /H_2O_2 ratio is an important key to achieve a higher removal efficiency (Hilles et al., 2016), 0.007, 0.03, and 0.06 M Na_2SO_4 concentrations were tested to identify the best concentration for which the highest NPs degradation could be reached. These tests were conducted for 90 min using the following conditions: 36 mA.cm^{-2} current density, initial NPs concentration of 10 mg/L, BDD as the anode, two pieces of CF cathodes, and air injection. The obtained NP removal efficiencies at different Na_2SO_4 concentrations are illustrated in Fig. 6a. After 40 min, the degradation efficiency of NPs with 0.03 M Na_2SO_4 was around 86%, while it was only 27% at 0.007 M Na_2SO_4. That can be ascribed to the greater production of $SO_4^{\bullet-}$ and $^{\bullet}OH$ in the solution due to the greater rate of $S_2O_8^{2-}$ electrogeneration at higher Na_2SO_4 concentration (Fig. 1c). As result, more $S_2O_8^{2-}$ is involved in Eq. (16). On the other hand, increasing the Na_2SO_4 concentration to 0.06 M had almost no effect in comparison to 0.03 M. That indicates the accumulated H_2O_2 under our electrolysis conditions was not sufficient to react with $S_2O_8^{2-}$. After 60 min the removal efficiencies reached 83.2 ± 4.9%, 88.9 ± 1.5%, and 89.0 ± 1.9% while imposing 0.007, 0.03, and 0.06 M Na_2SO_4, respectively.

Finally, to evaluate the robustness of our process, the initial concentration of NPs was increased to 20 mg/L. The results are shown in Fig. 6b. After 60 min of treatment, a high elimination rate was obtained reaching 93% of the NPs. These results indicate that increasing the concentration from 10 to 20 mg/L does not affect the performance of the process. The reduction rate obtained for a concentration of 10 mg/L was quite similar to that obtained with 20 mg/L after 60 min of treatment (88.9 ± 1.5% vs 93 ± 2.2%). Generally, the increase in the concentrations of pollutants has a negative effect on their elimination. In our case, the increase in the concentration of NPs increases its availability and the possibility of being oxidized by $^{\bullet}OH$ and $SO_4^{\bullet-}$. This indicates that the limit of pollutant concentration is not yet attained in our study (M. Murugananthan et al, 2008).

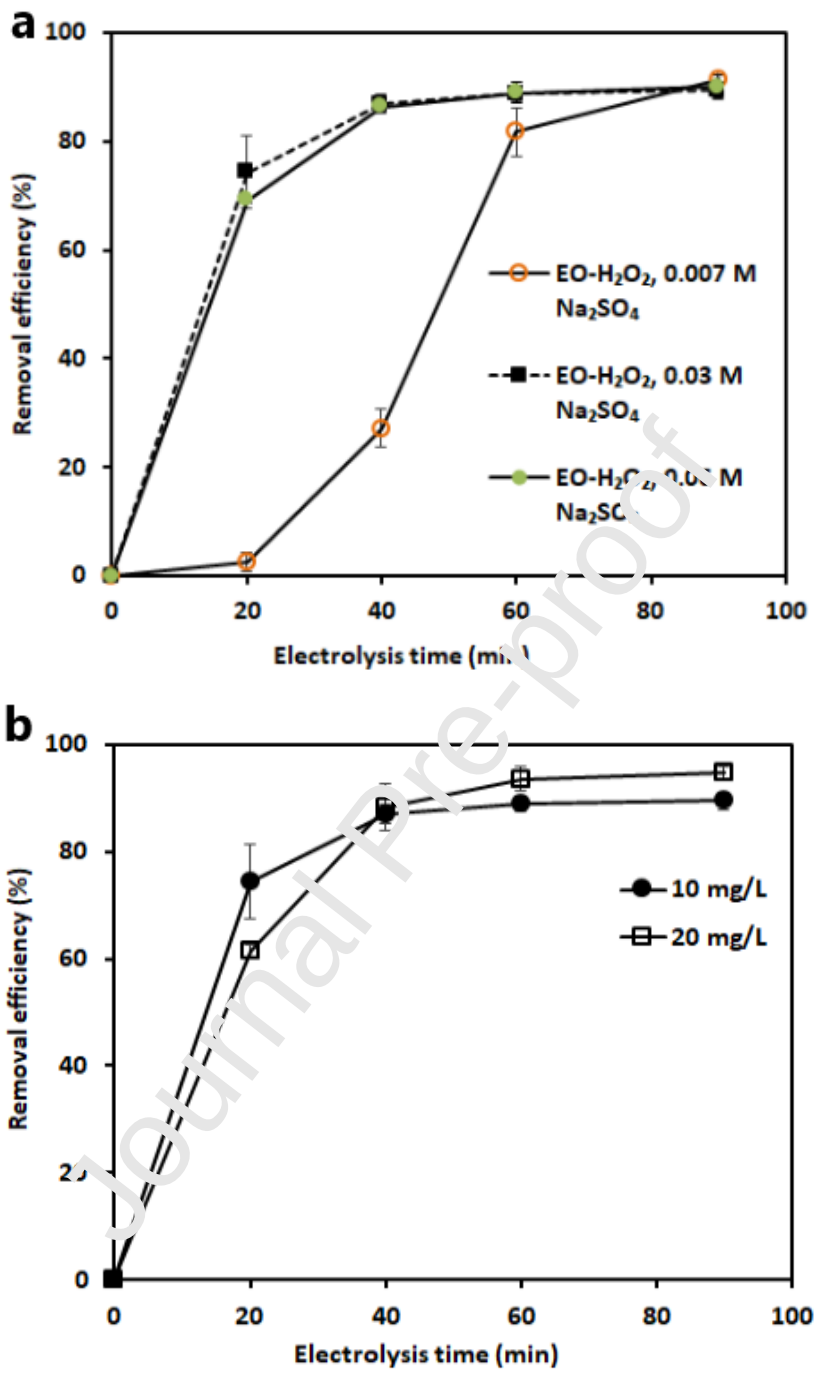

Fig. 6. The effect of (a) Na_2SO_4 concentration, and (b) initial NPs concentration on the NPs removal efficiency of EO-H_2O_2 process, current density = 36 mA.cm^{-2}, [Na_2SO_4] = 0.03 M, air injection, volume = 800 mL.

3.6. Analysis of NPs degradation by 3D EEM

The evolution of the dissolved organic matter in our solution was followed using high-resolution mass spectrometry and spectral (UV-VIS and fluorescence) analysis. This method has been reported as a useful tool for the characterization of dissolved and colloidal organic matter in water (Jacquin et al., 2017; Luo et al., 2019; Ouarda et al., 2020). In our study, the reactivity of nanoplastics organic matter (NPsOM) was monitored during electrolysis. The evolution of dissolved organic matter is shown in Fig. 7. 3D EEM analysis reveals the presence of three main peaks (a, b, and c) with high fluorophore intensity (FI). Peaks-a and b were located at the excitation/emission (Ex/Em) of 270-300/320 nm and 230/320 nm respectively. The peak-c was located at Ex/Em of 230/425 nm. Peaks a and b which are located at the same Em of 320 nm had been reported as aromatic-like peaks which may be associated with the benzene nucleus of PS in our study (Sheng and Yu, 2006; Yamashita and Tanoue, 2003). Peak-c is located in the region of Em > 380 nm represents humic acid-like substances which can be associated with surfactant alkoxyl substance in nanosphere standard (Chen et al., 2003; Luo et al., 2013; Wang et al., 2009). After 20 min electrolysis time, all the peaks were disintegrated. Peak-a has been blue-shifted compared with the peak at t_0 (Fig. 7c). Blueshift is associated with the decrease in the number of aromatic rings and conjugated bonds in a chain structure (Coble, 1996; Swietlik et al., 2004). After 40 min of electrolysis, FI of peak-b and c decreased significantly from 666 to 295, while peak-a decreased from approximately 295 to 146 (Fig. 7d). Peak-a got disappeared after 60 min of treatment (Fig. 7e). However, peak-b and c were further decayed. After 60 min, the synthetic NPs solution was weakly fluorescent (Fig. 7e). Thus, the decrease in the fluorescence signal could be attributed only to the elimination of NPs under the action of by $^{\bullet}OH$ and $SO_4^{\bullet-}$ radicals.

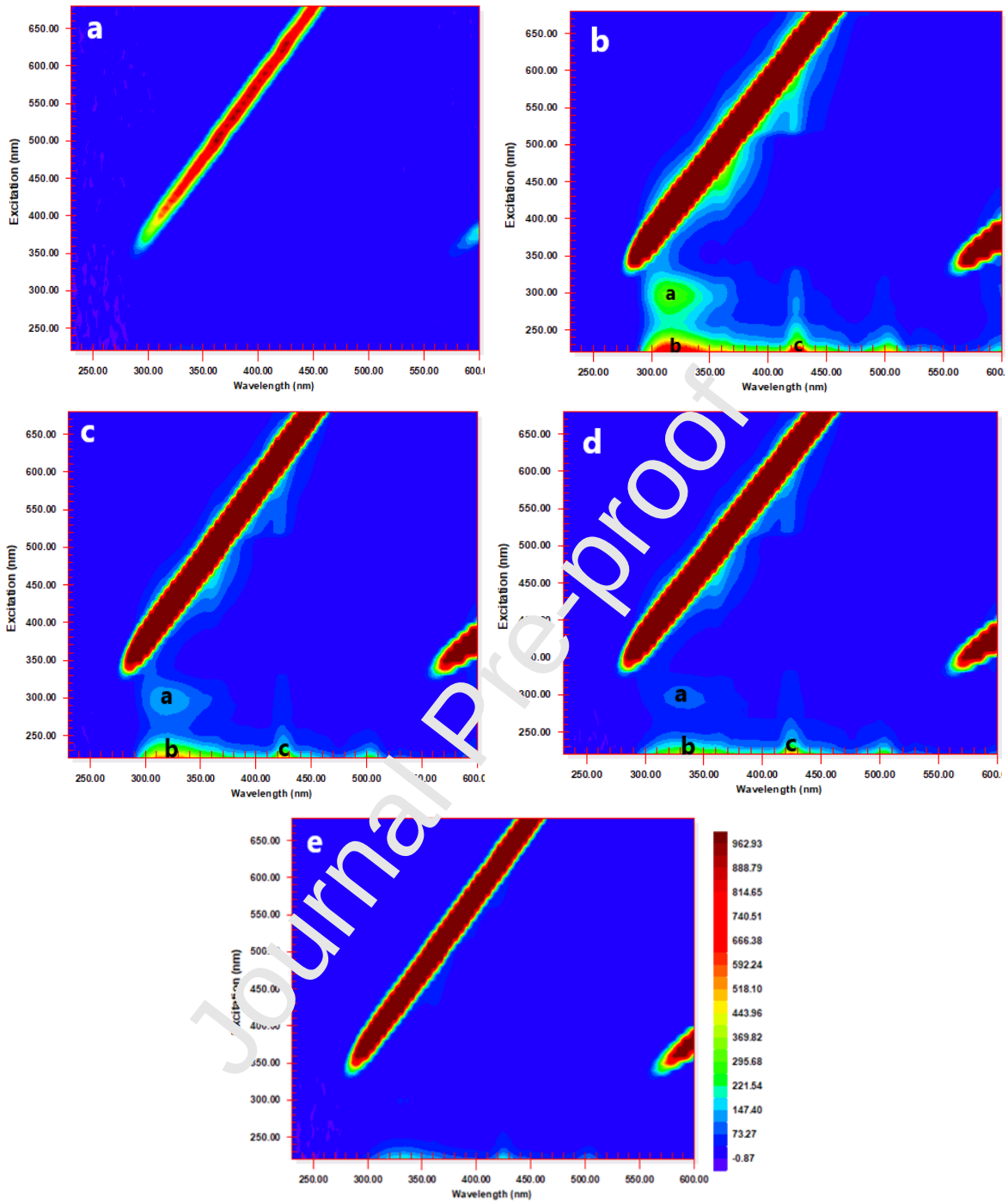

Fig. 7. Evolution of 3D EEM fluorescence spectra while applying EO-H_2O_2 process for the treatment PS NP, 0.007 M Na_2SO_4 treatment : a) desionized water, b) NPs synthetic solution at t = 0 min, c) t = 20 min, d) t = 40 min, e) t = 60 min.

3.7. Economic analysis

The economical aspect and especially the energy consumption expressed as $kWh.m^{-3}$ is an important concern in EAOPs. Therefore, the EO and EO-H_2O_2 treatment costs of PS NPs (including only chemical consumption and energy consumption) at the optimal conditions were estimated. the calculated costs analysis data are presented in Table 2. Energy consumption (in terms of $kWh.m^{-3}$) was calculated. A percentage of NPs degradation of 86.8 ± 1.8% was recorded after 0.67 h of electrolysis time in the presence of 0.03 M Na_2SO_4 using the EO-H_2O_2 process. By comparison, to reach approximately the same level of NPs degradation (80.4 ± 0.93%), a period of electrolysis of 6 h was required using the EO process. In addition, using two pieces of CF as cathodes in the EO-H_2O_2 process, an average 8.6 V potential difference between electrodes was recorded. By comparison, an average value of 16.2 V was recorded for the EO process (using one piece of Ti as the cathode). Accordingly, the energy consumption of 363.8 $kWh.m^{-3}$ was obtained for the EO process compared to only 21.6 $kWh.m^{-3}$ using the EO-H_2O_2 process. Thus, the operating cost could be reduced from 22.1 $US.m^{-3}$ (by using the EO process) to 2.6 $US.m^{-3}$ (by using the EO-H_2O_2 process).

Table 2. Cost analysis of NPs removal using EO, EO-H_2O_2 processes at 0.007 and 0.03 M Na_2SO_4.

	EO (0.007 M Na_2SO_4)	**EO-H_2O_2/$S_2O_8^{2-}$ (0.007 M Na_2SO_4)**	**EO-H_2O_2/$S_2O_8^{2-}$ (0.03 M Na_2SO_4)**
Time (h)	6	1	0.67
Optimal removal (%)	80.4 ± 0.93	83.2 ± 1.5	86.8 ± 1.8
T (V)	16.2	8.7	8.6
Energy consumption ($kWh.m^{-3}$)	363.8	32.8	21.6
Na_2SO_4 cost ($US.m^{-3}$)	0.3	0.3	1.3
Energy cost ($US.m^{-3}$)	21.8	1.9	1.6
Operating cost ($US.m^{-3}$)	22.1	2.3	2.8

Conclusion

The electrochemical process is a feasible technology for the treatment of water contaminated by NPs. The analysis of ROSs in EO-H_2O_2 process showed that H_2O_2 concentrations up to 24.2 × 10^{-3} M could be generated. The generated ROSs using EO-H_2O_2 process increased the NPs degradation around 2.6 times in comparison to EO process. 86.8 % ± 1.8 % NPs degradation efficiency was obtained by EO-H_2O_2 process at the optimized current density of 36 mA.cm^{-2} in 40 min. 3D EEM fluorescence analysis also confirmed the degradation of NPs in EO-H_2O_2 process. TOC analysis revealed that the degraded NPs were mainly mineralized (TOC removal up to 76.5 ± 0.64%) and transformed into CO_2 and H_2O. Finally, an economic analysis of EO-H_2O_2 process showed that it has an operating cost of 2.3 $US.$m^{-3}$, which is around 10 times less than the cost recorded for EO process. The current work showed the ROSs could have a great contribution in the degradation of NPs in water and significantly reduce the cost of process. However, further research is required to make the process faster and more economical. Prior treatment with nanofiltration followed by electrochemical degradation technique could form the basis process capable of effectively removing NPs from many waters (drinking water, municipal and industrial wastewaters).

Acknowledgments

The authors would like to acknowledge the financial support from the Fonds de recherche du Québec-Nature et technologies (FRQNT), the CREATE-TEDGIEER program, the National Sciences and Engineering Research Council of Canada (NSERC), and the Canadian Francophonie Scholarship Program.

References

Ali MI, Ahmed S, Robson G, Javed I, Ali N, Atiq N, et al. Isolation and molecular characterization of polyvinyl chloride (PVC) plastic degrading fungal isolates. J Basic Microbiol 2014; 54: 18-27.

Ariza-Tarazona MC, Villarreal-Chiu JF, Barbieri V, Siligardi C, Cedillo-González EI. New strategy for microplastic degradation: Green photocatalysis using a protein-based porous N-TiO_2 semiconductor. Ceram. Int. 2019; 45: 9618-9624.

Badellino C, Rodrigues CA, Bertazzoli R. Oxidation of pesticides by in situ electrogenerated hydrogen peroxide: study for the degradation of 2,4-dichlorophenoxyacetic acid. J Hazard Mater 2006; 137: 856-64.

Bañuelos JA, García-Rodríguez O, El-Ghenymy A, Rodríguez-Valadez FJ, Godínez LA, Brillas E. Advanced oxidation treatment of malachite green dye using a low cost carbon-felt air-diffusion cathode. J. Environ. Chem. Eng. 2016; 4: 2066-2075.

Barreto JPdP, Araujo KCdF, de Araujo DM, Martinez-Huitle CA. Effect of sp3/sp2 Ratio on Boron Doped Diamond Films for Producing Persulfate. ECS Electrochem. Lett. 2015; 4: E9-E11.

Cai H, Xu EG, Du F, Li R, Liu J, Shi H. Analysis of environmental nanoplastics: Progress and challenges. Chem. Eng. J. 2021; 410.

Cai J, Zhou M, Liu Y, Savall A, Groenen Serrano K. Indirect electrochemical oxidation of 2,4-dichlorophenoxyacetic acid using electrochemically-generated persulfate. Chemosphere 2018; 204: 163-169.

Canizares P, Lobato J, Paz R, Rodrigo MA, Saez C. Electrochemical oxidation of phenolic wastes with boron-doped diamond anodes. Water Res 2005; 39: 2687-703.

Chen W, Westerhoff P, LEenheer JA, Booksh K. Fluorescence excitation-emission matrix regional integration to quantify spectra for dissolved organic Matter. Environ. Sci. Technol. 2003; 37: 5701-5710.

Chen Z, Huang Z, Liu J, Wu E, Zheng Q, Cui L. Phase transition of Mg/Al-flocs to Mg/Al-layered double hydroxides during flocculation and polystyrene nanoplastics removal. J Hazard Mater 2021; 406: 124697.

Ciríaco L, Anjo C, Correia J, Pacheco MJ, Lopes A. Electrochemical degradation of Ibuprofen on Ti/Pt/PbO_2 and Si/BDD electrodes. Electrochim. Acta 2009; 54: 1464-1472.

Coble PG. Characterization of marine and terrestrial DOM in seawater using excitation-emission matrix spectroscopy. Marine Chemistry 51 1996; 51: 325-346.

Cotillas S, Llanos J, Rodrigo MA, Cañizares P. Use of carbon felt cathodes for the electrochemical reclamation of urban treated wastewaters. Appl. Catal. B: Environ 2015; 162: 252-259.

da Costa JP, Santos PSM, Duarte AC, Rocha-Santos T. (Nano)plastics in the environment - Sources, fates and effects. Sci Total Environ 2016; 566-567: 15-26.

Daghrir R[a, 1], Drogui P, Dimboukou-Mpira A, El Khakani MA. Photoelectrocatalytic degradation of carbamazepine using Ti/TiO_2 nanostructured electrodes deposited by means of a pulsed laser deposition process. Chemosphere 2013; 93: 2756-66.

Davis J, Baygents JC, Farrell J. Understanding Persulfate Production at Boron Doped Diamond Film Anodes. Electrochim. Acta 2014; 150: 68-74.

De Villiers S. Short communication: Microfibre pollution hotspots in river sediments adjacent to South Africa's coastline. Water SA 2019; 45.

Deng Y, Ezyske CM. Sulfate radical-advanced oxidation process (SR-AOP) for simultaneous removal of refractory organic contaminants and ammonia in landfill leachate. Water Res 2011; 45: 6189-94.

Deng Y, Zhao R. Advanced Oxidation Processes (AOPs) in Wastewater Treatment. Curr. Pollut. Rep. 2015; 1: 167-176.

Divyapriya G, Nidheesh PV. Electrochemically generated sulfate radicals by boron doped diamond and its environmental applications. Curr. Opin. Solid State Mater. Sci 2021; 25.

Dominguez-Jaimes LP, Cedillo-Gonzalez EI, Luevano-Hipolito E, Acuna-Bedoya JD, Hernandez-Lopez JM. Degradation of primary nanoplastics by photocatalysis using different anodized TiO_2 structures. J Hazard Mater 2021; 413: 125452.

Dos Santos AJ, Brillas E, Cabot PL, Sires I. Simultaneous persulfate activation by electrogenerated H_2O_2 and anodic oxidation at a boron-doped diamond anode for the treatment of dye solutions. Sci Total Environ 2020; 747: 141541.

Durán FE, de Araújo DM, do Nascimento Brito C, Santos EV, Ganiyu SO, Martínez-Huitle CA. Electrochemical technology for the treatment of real washing machine effluent at pre-pilot plant scale by using active and non-active anodes. J. Electroanal. Chem. 2018; 818: 216-222.

Ekvall MT, Lundqvist M, Kelpsiene E, Šileikis E, Gunnarsson SB, Cedervall T. Nanoplastics formed during the mechanical breakdown of daily-use polystyrene products. Nanoscale Adv. 2019; 1: 1055-1061.

Enfrin M, Dumee LF, Lee J. Nano/microplastics in water and wastewater treatment processes - Origin, impact and potential solutions. Water Res 2019; 161: 621-638.

Entezari MH, Kruus P. Effect of frequency on sonochemical reactions. I: Oxidation of iodide. Ultrason Sonochem 1994; 1: 75-79.

Fan G, Cang L, Fang G, Qin W, Ge L, Zhou D. Electrokinetic delivery of persulfate to remediate PCBs polluted soils: effect of injection spot. Chemosphere 2014; 117: 410-8.

Ganiyu SO, Martínez-Huitle CA. Nature, Mechanisms and Reactivity of Electrogenerated Reactive Species at Thin-Film Boron Doped Diamond (BDD) Electrodes During Electrochemical Wastewater Treatment. ChemElectroChem 2019; 6: 2379-2392.

García-Gómez C, Drogui P, Zaviska F, Seyhi B, Gortáres-Moroyoqui P, Buelna G, et al. Experimental design methodology applied to electrochemical oxidation of carbamazepine using Ti/PbO$_2$ and Ti/BDD electrodes. J. Electroanal. Chem. 2014; 732: 1-10.

Garcia-Segura S, El-Ghenymy A, Centellas F, Rodríguez RM, Arias C, Garrido JA, et al. Comparative degradation of the diazo dye Direct Yellow 4 by electro-Fenton, photoelectro-Fenton and photo-assisted electro-Fenton. J. Electroanal. Chem. 2012; 681: 36-43.

Gigault J, Halle AT, Baudrimont M, Pascal PY, Gauffre F, Phi TL, et al. Current opinion: What is a nanoplastic? Environ Pollut 2018; 235: 1030-1034.

González-Pleiter M, Tamayo-Belda M, Pulido-Reyes G, Amariei G, Leganés F, Rosal R, et al. Secondary nanoplastics released from a biodegradable microplastic severely impact freshwater environments. Environ. Sci. Nano 2019; 6: 1382-1392.

Guitaya L, Drogui P, Blais JF. In situ reactive oxygen species production for tertiary wastewater treatment. Environ Sci Pollut Res Int 2015; 22: 7025-36.

Hernandez LM, Yousefi N, Tufenkji N. Are There Nanoplastics in Your Personal Care Products? Environ. Sci. Technol. Lett. 2017; 4: 280-285.

Hilles AH, Abu Amr SS, Hussein RA, Arafa AI, El-Sebaie OD. Effect of persulfate and persulfate/H_2O_2 on biodegradability of an anaerobic stabilized landfill leachate. Waste Manag 2015; 44: 172-7.

Hilles AH, Abu Amr SS, Hussein RA, El-Sebaie OD, Arafa AI. Performance of combined sodium persulfate/H_2O_2 based advanced oxidation process in stabilized landfill leachate treatment. J Environ Manage 2016; 166: 493-8.

Ignasi S, Enric B, Giacomo C, Marco P. Comparative depollution of mecoprop aqueous solutions by electrochemical incineration using BDD and PbO_2 as high oxidation power anodes. J. Electroanal. Chem. 2008; 613: 151–159.

Ishibashi K-i, Fujishima A, Watanabe T, Hashimotoa K. Quantum yields of active oxidative species formed on TiO_2 photocatalyst. Journal of Photochemistry and Photobiology A: Chemistry 2000; 134: 139–142.

Jacquin C, Lesage G, Traber J, Pronk W, Heran M. Three-dimensional excitation and emission matrix fluorescence (3DEEM) for quick and pseudo-quantitative determination of protein- and humic-like substances in full-scale membrane bioreactor (MBR). Water Res 2017; 118: 82-92.

Kang J, Zhou L, Duan X, Sun H, Ao Z, Wang S. Degradation of Cosmetic Microplastics via Functionalized Carbon Nanosprings. Matter 2019; 1: 745-758.

Karimi Estahbanati MR, Kiendrebeogo M, Khosravanipour Mostafazadeh A, Drogui P, Tyagi RD. Treatment processes for microplastics and nanoplastics in waters: State-of-the-art review. Mar Pollut Bull 2021a; 168: 112374.

Karimi Estahbanati MR, Kong XY, Eslami A, Soo HS. Current Developments in the Chemical Upcycling of Waste Plastics Using Alternative Energy Sources. ChemSusChem 2021b; 14: 4152-4166.

Karimi Estahbanati MR, Kumar S, Khajvand M, Drogui P, Tyagi RD. Environmental Impacts of Recovery of Resources From Industrial Wastewater. Biomass, Biofuels, Biochemicals. Elsevier, 2021c; pp. 121-162.

Kashiwada S. Distribution of nanoparticles in the see-through medaka (Oryzias latipes). Environ Health Perspect 2006; 114: 1697-702.

Kelly MR, Lant NJ, Kurr M, Burgess JG. Importance of Water-Volume on the Release of Microplastic Fibers from Laundry. Environ Sci Technol 2019; 53: 11735-11744.

Khataee AR, Safarpour M, Zarei M, Aber S. Electrochemical generation of H_2O_2 using immobilized carbon nanotubes on graphite electrode fed with air: Investigation of operational parameters. J. Electroanal. Chem. 2011; 659: 63-68.

Kiendrebeogo M, Karimi Estahbanati MR, Khosravanipour Mostafazadeh A, Drogui P, Tyagi RD. Treatment of microplastics in water by anodic oxidation: A case study for polystyrene. Environ Pollut 2021; 269: 116168.

Koda S, Kimura T, Kondo T, Mitome H. A standard method to calibrate sonochemical efficiency of an individual reaction system. Ultrason Sonochem. 2003; 10: 149-156.

Komtchou S, Dirany A, Drogui P, Bermond A. Removal of carbamazepine from spiked municipal wastewater using electro-Fenton process. Environ Sci Pollut Res Int 2015; 22: 11513-25.

Koziara JM, Lockman PR, Allen DD, Mumper RJ. In Situ Blood–Brain Barrier Transport of Nanoparticles. Pharm. Res. 2003; Vol. 20, No. 11.

Lan Y, Coetsier C, Causserand C, Groenen Serrano K. On the role of salts for the treatment of wastewaters containing pharmaceuticals by electrochemical oxidation using a boron doped diamond anode. Electrochim. Acta 2017; 231: 309-318.

Li Y, Zhang Y, Xia G, Zhan J, Yu G, Wang Y. Evaluation of the technoeconomic feasibility of electrochemical hydrogen peroxide production for decentralized water treatment. Front. Environ. Sci. Eng. 2020; 15.

Lin CK, Bashir MJ, Abu Amr SS, Sim LC. Post-treatment of palm oil mill effluent (POME) using combined persulphate with hydrogen peroxide ($S_2O_8^{2-}/H_2O_2$) oxidation. Water Sci Technol 2016; 74: 2675-2682.

Lithner D, Larsson A, Dave G. Environmental and health hazard ranking and assessment of plastic polymers based on chemical composition. Sci Total Environ 2011; 409: 3309-24.

Liu L, Fokkink R, Koelmans AA. Sorption of polycyclic aromatic hydrocarbons to polystyrene nanoplastic. Environ Toxicol Chem 2016; 35: 1650-5.

Luo H, Liu C, He D, Xu J, Sun J, Li J, et al. Environmental behaviors of microplastics in aquatic systems: A systematic review on degradation, adsorption, toxicity and biofilm under aging conditions. J Hazard Mater 2021; 423: 126915.

Luo H, Xiang Y, He D, Li Y, Zhao Y, Wang S, et al. Leaching behavior of fluorescent additives from microplastics and the toxicity of leachate to Chlorella vulgaris. Sci Total Environ 2019; 678: 1-9.

Luo K, Yang Q, Li XM, Chen HB, Liu X, Yang GJ, et al. Novel insights into enzymatic-enhanced anaerobic digestion of waste activated sludge by three-dimensional excitation and emission matrix fluorescence spectroscopy. Chemosphere 2013; 91: 579-85.

Ma Y, Huang A, Cao S, Sun F, Wang L, Guo H, et al. Effects of nanoplastics and microplastics on toxicity, bioaccumulation, and environmental fate of phenanthrene in fresh water. Environ Pollut 2016; 219: 166-173.

Mahon AM, O'Connell B, Healy MG, O'Connor I, Officer R, Nash R, et al. Microplastics in sewage sludge: effects of treatment. Environ Sci Technol 2017; 51: 810-818.

Marselli B, Garcia-Gomez J, Michaud PA, Rodrigo MA, Comninellis C. Electrogeneration of Hydroxyl Radicals on Boron-Doped Diamond Electrodes. J. Electrochem. Soc. 2003; 150.

Martínez-Huitle CA, Panizza M. Electrochemical oxidation of organic pollutants for wastewater treatment. Curr. Opin. Electrochem 2018; 11: 62-71.

Martínez-Huitle CA, Quiroz MA, Comninellis C, Ferro S, Battisti AD. Electrochemical incineration of chloranilic acid using Ti/IrO_2, Pb/PbO_2 and Si/BDD electrodes. Electrochim. Acta 2004; 50: 949-956.

Martinez-Huitle CA, Rodrigo MA, Sires I, Scialdone O. Single and coupled electrochemical processes and reactors for the abatement of organic water pollutants: A critical review. Chem Rev 2015; 115: 13362-407.

Matta R, Tlili S, Chiron S, Barbati S. Removal of carbamazepine from urban wastewater by sulfate radical oxidation. Environ. Chem. Lett. 2010; 9: 347-353.

Miao F, Liu Y, Gao M, Yu X, Xiao P, Wang M, et al. Degradation of polyvinyl chloride microplastics via an electro-Fenton-like system with a TiO_2/graphite cathode. J Hazard Mater 2020; 399: 123023.

Miyake Y, Tokumura M, Wang Q, Amagai T, Horii Y. Rate of hexabromocyclododecane decomposition and production of brominated polycyclic aromatic hydrocarbons during combustion in a pilot-scale incinerator. J Environ Sci (China) 2017; 61: 91-96.

Muff J, Bennedsen LR, Søgaard EG. Study of electrochemical bleaching of p-nitrosodimethylaniline and its role as hydroxyl radical probe compound. J. Appl. Electrochem. 2011; 41: 599-607.

Murray A, Örmeci B. Removal effectiveness of Nanoplastics (<400 nm) with separation processes used for water and wastewater treatment. Water 2020; 12.

Nidheesh PV, Rajan R. Removal of rhodamine B from a water medium using hydroxyl and sulphate radicals generated by iron loaded activated carbon. RSC Advances 2016; 6: 5330-5340.

Niu T, Cai J, Shi P, Zhao G. Unique electrochemical system for in situ SO_4^- generation and pollutants degradation. Chem. Eng. J. 2020; 386.

Ouarda Y, Trellu C, Lesage G, Rivallin M, Drogui P, Cretin M. Electro-oxidation of secondary effluents from various wastewater plants for the removal of acetaminophen and dissolved organic matter. Sci Total Environ 2020; 738: 140352.

Özcan A, Şahin Y, Savaş Koparal A, Oturan MA. Carbon sponge as a new cathode material for the electro-Fenton process: Comparison with carbon felt cathode and application to degradation of synthetic dye basic blue 3 in aqueous medium. J. Electroanal. Chem. 2008; 616: 71-78.

Paco A, Duarte K, da Costa JP, Santos PSM, Pereira R, Pereira ME, et al. Biodegradation of polyethylene microplastics by the marine fungus Zalerion maritimum. Sci Total Environ 2017; 586: 10-15.

Panizza M, Cerisola G. Application of diamond electrodes to electrochemical processes. Electrochim. Acta 2005; 51: 191-199.

Phonsy PD, Anju SG, Jyothi KP, Suguna Y, Yesodharan EP. Semiconductor mediated photocatalytic degradation of plastics and recalcitrant organic pollutants in water: effect of additives and fate of insitu formed H_2O_2. J. Adv. Oxid. Technol. 2015; 18: 85-97.

Salmerón I, Plakas KV, Sirés I, Oller I, Maldonado MI, Karabelas AJ, et al. Optimization of electrocatalytic H_2O_2 production at pilot plant scale for solar-assisted water treatment. Appl. Catal. B: Environ. 2019; 242: 327-336.

Sanni I, Karimi Estahbanati MR, Carabin A, Drogui P. Coupling electrocoagulation with electro-oxidation for COD and phosphorus removal from industrial container wash water. Sep. Purif. Technol. 2021: 119992.

Serrano K, Michaud PA, Comninellis, Savall A. Electrochemical preparation of peroxodisulfuric acid using boron doped diamond thin film electrodes. Electrochim. Acta 2002; 48: 431- 436.

Sheng GP, Yu HQ. Characterization of extracellular polymeric substances of aerobic and anaerobic sludge using three-dimensional excitation and emission matrix fluorescence spectroscopy. Water Res 2006; 40: 1233-9.

Sigler PB, MAster BJ. Hydrogen peroxide-induced ce*(III)-ce(IV) exchange syste. J Am Chem Soc 1957; 79: 6353-6357.

Simonsen ME, Muff J, Bennedsen LR, Kowalski KP, Søgaard EG. Photocatalytic bleaching of p-nitrosodimethylaniline and a comparison to the performance of other AOP technologies. Journal of Photochemistry and Photobiology A: Chemistry 2010; 216: 244-249.

Sires I, Brillas E, Oturan MA, Rodrigo MA, Panizza M. Electrochemical advanced oxidation processes: today and tomorrow. A review. Environ Sci Pollut Res Int 2014; 21: 8336-67.

Smit W, Hoogland JG. The mechanism of the anodic formation the of the peroxodisulphate ion on platinum-I. Establishment of participing anion. Electrochim. Acta 1971a; 16: 1-18.

Smit W, Hoogland JG. The mechanism of the anodic formationthe of the peroxodisulphate ion on platinum-II. Time dependence of the anode potential. Eectrochimica Acta 1971b; 16: 821 to 831.

Stichnothe H, Kellera A, Thöming J, Lohmann N, Calmano W. Reduction of tributyltin (TBT) and other organic pollutants of concern in contaminated sediments by means of an electrochemical oxidation. Acta hydrochim. hydrobiol. 2002; 30: 87-93.

Swietlik J, Dabrowska A, Raczyk-Stanislawiak U, Nawrocki J. Reactivity of natural organic matter fractions with chlorine dioxide and ozone. Water Res 2004; 38: 547-58.

Tsitonaki A, Petri B, Crimi M, MosbÆK H, Siegrist RL, Bjerg PL. In situ chemical oxidation of contaminated soil and groundwater using persulfate: A review. Crit. Rev. Environ. Sci. Technol. 2010; 40: 55-91.

Wacławek S, Lutze HV, Grübel K, Padil VVT, Černík M, Dionysiou DD. Chemistry of persulfates in water and wastewater treatment. A review. Chem. Eng. J. 2017; 330: 44-62.

Wang S, Liu M, Wang J, Huang J, Wang J. Polystyrene nanoplastics cause growth inhibition, morphological damage and physiological disturbance in the marine microalga Platymonas helgolandica. Mar Pollut Bull 2020; 158: 111403.

Wang Z, Wu Z, Tang S. Characterization of dissolved organic matter in a submerged membrane bioreactor by using three-dimensional excitation and emission matrix fluorescence spectroscopy. Water Res 2009; 43: 1533-40.

White KL. An overview of immunotoxicology and carcinogenic polycyclic aromatic hydrocarbons. Environmental Carcinogenesis Reviews 1986; 4: 163-202.

Wojnarovits L, Takacs E. Rate constants of sulfate radical anion reactions with organic molecules: A review. Chemosphere 2019; 220: 1014-1032.

Xiang Q, Yu J, Wong PK. Quantitative characterization of hydroxyl radicals produced by various photocatalysts. J Colloid Interface Sci 2011; 357: 163-7.

Yamashita Y, Tanoue E. Chemical characterization of protein-like fluorophores in DOM in relation to aromatic amino acids. Marine Chemistry 2003; 82: 255-271.

Yassine O, Bhagyashree T, Antonin A, Marc-Antoine V, Sokhna D, Ndiaye,, Patrick D, et al. Synthetic hospital wastewater treatment by coupling submerged membrane bioreactor and electrochemical advanced oxidation process: Kinetic study and toxicity assessment. Chemosphere 2018; 193: 160-169.

Yue J, Epstein AJ, MacDiarmid AG. Sulfonic acid ring-substituted polyaniline, a self-doped conducting polymer. Mol. Cryst. Liq. Cryst. 1990; 189: 255-261.

Zhou W, Gao J, Kou K, Meng X, Wang Y, Ding Y, et al. Highly efficient H_2O_2 electrogeneration from O_2 reduction by pulsed current: Facilitated release of H_2O_2 from porous cathode to bulk. J. Taiwan Inst. Chem. Engrs. 2018; 83: 59-63.

Zhou W, Meng X, Gao J, Alshawabkeh AN. Hydrogen peroxide generation from O_2 electroreduction for environmental remediation: A state-of-the-art review. Chemosphere 2019; 225: 588-607.

AUTHORSHIP STATEMENT

Marthe Kiendrebeogo: Conceptualization, Methodology, Validation, Investigation, Writing - Original Draft, Visualization.

M.R. Karimi Estahbanati: Conceptualization, Methodology, Validation, Writing - Original Draft, Writing - Review & Editing, Supervision.

Yassine Ouarda: Conceptualization, Methodology, Validation, Writing - Review & Editing.

Patrick Drogui: Conceptualization, Methodology, Validation, Investigation, Resources, Writing - Original Draft, Writing - Review & Editing, Supervision, Project administration, Funding acquisition.

RD. Tyagi: Conceptualization, Methodology, Validation, Writing - Review & Editing.

Declaration of interests

☐ The authors declare that they have no known competing financial interests or personal relationshipsthat could have appeared to influence the work reported in this paper.

☒The authors declare the following financial interests/personal relationships which may be consideredas potential competing interests:

Fonds de recherche du Québec – Nature et technologies (FRQNT)
CREATE-TEDGIEER program

National Sciences and Engineering Research Council of Canada (NSERC)
Canadian Francophonie Scholarship Program

Patrick DROGUI

Graphical abstract

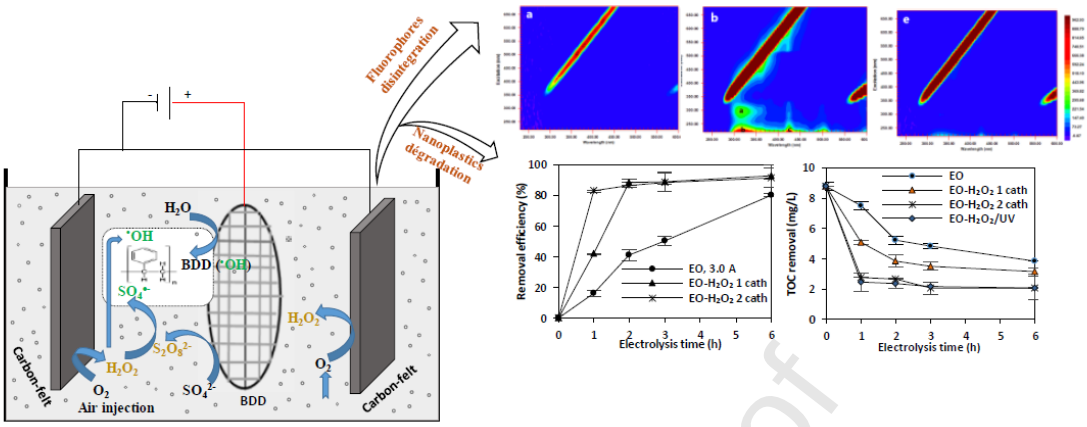

HIGHLIGHTS

- $^{\bullet}OH$, $S_2O_8^{2-}$, and H_2O_2 were generated during the electrooxidation (EO) process.
- Role of reactive oxygen species in EO of nanoplastics (NPs) in water was studied.
- 86.8% NPs degradation efficiency was obtained only after 0.67 h.
- $S_2O_8^{2-}/H_2O_2$ activation increased the rate of NPs degradation 2.6 times.
- 3D EEM fluorescence analysis confirmed the degradation of NPs.